59th ILMENAU SCIENTIFIC COLLOQUIUM
Technische Universität Ilmenau, 11 — 15 September 2017
URN: urn:nbn:de:gbv:ilm1-2017iwk-050:5

VIBRISSA-BASED DESIGN OF TAPERED TACTILE SENSORS FOR OBJECT SENSING

Carsten Behn / Lisa Ackermann / Christoph Will / Thomas Helbig / Joachim Steigenberger

Technical Mechanics Group, Biomechatronics Group & Institute of Mathematics
Technische Universität Ilmenau
Max-Planck-Ring 12, 98693 Ilmenau, Germany
carsten.behn@tu-ilmenau.de

DEDICATION

The authors like to thank and to dedicate this paper at hand to their cherished and in July 2017 deceased colleague Mrs. Danja Voges. R.I.P. Danja – you were a very special person to us. We miss you badly.

ABSTRACT

Numerous mammals possess whiskers (tactile hairs, also known as vibrissae) to explore their environment. These complex mechano-sensitive vibrissae are located, e.g. in the snout region (mystacial vibrissae). Because of the deformation of the vibrissa by contact with objects and obstacles, the animal gets additional information about the environment. Despite different morphology of animal vibrissae (e.g., cylindrically or conically shaped, pre-curved, multi-layer structure), these biological tactile hairs are modeled in a mechanical way to develop and analyze models concerning their bending behavior with a glance to get hints for a technical implementation as a technical sensor. At first, we investigate the bending behavior of cylindrically shaped and tapered rods which are one-sided clamped and are under the load of an external force, using the Euler-Bernoulli non-linear bending theory. Then, a quasi-static sweep of these rods along various obstacle profiles is used for an obstacle profile reconstruction procedure. While scanning the object, the clamping reactions are determined, which are the only observables an animal relies on in biology. In plotting these observables and using them in a reconstruction algorithm to determine the scanned contour, we try to identify special features in dependence on the different geometries of the rods. The clamping reactions tremendously depend on the form and position of the profile which is shown in several numerical simulations.

Index Terms— tactile sensor, bio-inspired sensor, animal vibrissa, tapered shape, object contour reconstruction.

1. INTRODUCTION

On the body of mammals a tactile sensory organ with incomparable abilities can be found -– the so-called *sinus hairs*. Despite existing differences regarding musculature (see Fig. 1-left) and localization, they are synonymously also known as *vibrissae* or *whiskers* [18]. Depending on their localization on the body [21] they are used for different tasks like object recognition [6], object discrimination [7, 8] and perception of flow [8, 30] as well as for social behavior [1, 15]. The hair shaft itself has no receptors along its length [9]. Following the concept of a biomechatronic system [27], it can be seen as infector and transmission for all tactile stimuli arising along the shaft. Different studies try to explain this transmission to the mechanoreceptors in the follicle (see Fig. 1-right) from a mechanical point of view [2, 10, 16, 17].
Therefore, exact descriptions of the geometry as well as material parameters of the hair shaft are necessary. Studies have shown that the hair shaft is a thin, long and pliable truncated cone with a high aspect ratio of length to diameter [4, 24, 29]. Especially the tapered structure (see Fig. 2) has an important role for object sensing [12, 26].
This assertion is the starting point of the paper at hand: analytical investigations of the tapered shape on the bending behavior of artificial sinus hairs for prototypes in context of object sensing – from the mechanical point of view.

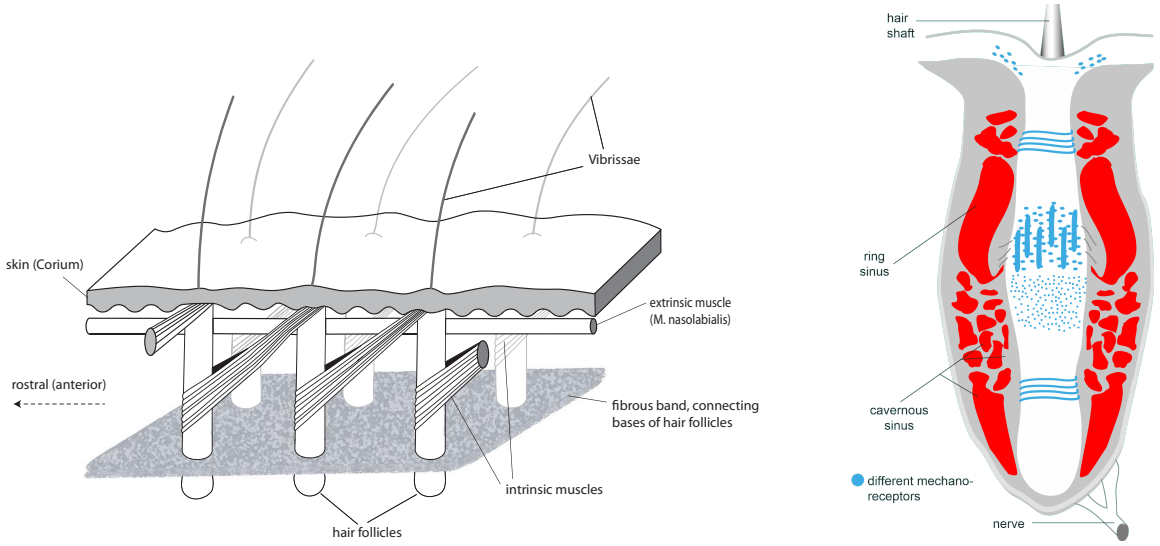

Figure 1. Sinus hairs of mammals: Left – schematic drawing of neighboring follicles [3]; Right - schematic overview of the basic elements of the follicle-sinus-complex with receptors (blue) [11].

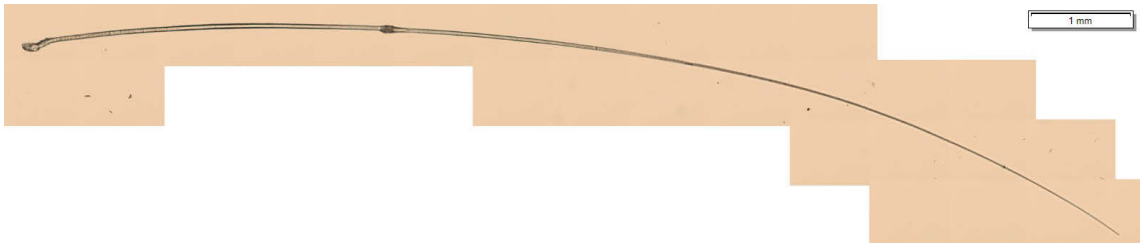

Figure 2. Stitched overview of a carpal sinus hair taken with an Olympus® $BX51$ system microscope at a magnification of 10x.

In literature, there are several investigations concerning the bending behavior of rods – serving as models for tactile sensors:

- In early works [5, 14, 23], first (mathematical) models describing large deflections of Euler-Bernoulli rods were analyzed, without any concern to artificial sensors.
- Further works, focussing the bending behavior of rods in context to animal vibrissae, are [13, 19, 22], but with a restriction to cylindrical rods.
- A lot of other works focus the dynamical bending behavior of rods, e.g. see [16], more precisely, the investigation – primary in a numerical way – of the natural frequencies of straight rods.
- First works, analyzing the bending behavior of conically shaped rods in context of bio-inspired sensors are [17, 20, 28], but they are limited to multi-body systems or finite element models, which shall approximate the bending behavior of rods (have to be modeled as a continuum in mechanics).

Therefore, we focus on the analytical modeling of conically shaped rods in continuum mechanics. The paper is arranged as follows: Section 2 presents preliminary studies concerning the static bending behavior of tapered artificial sensors, whose information is then used for the object contour detection algorithm in Section 3. The paper ends up with a conclusion and an outlook on future work.

2. PRELIMINARY STATIC BENDING STUDIES

Starting point is the description of a plane curve (w.l.o.g., in x-y-plane) in natural coordinates – in dependence on the arc length s, parameterized by the slope angle $\varphi(s)$:

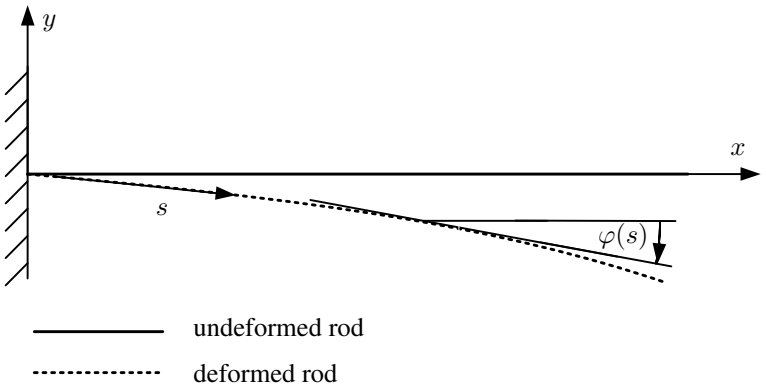

Figure 3. Illustration of slope angle φ and arc lenght s.

$$\left.\begin{aligned} \frac{dx(s)}{ds} &= \cos\Big(\varphi(s)\Big) \\ \frac{dy(s)}{ds} &= \sin\Big(\varphi(s)\Big) \\ \frac{d\varphi(s)}{ds} &= \kappa(s) = \frac{M_{bz}(s)}{E\, I_z(s)} \end{aligned}\right\} \tag{1}$$

With a glance to Fig. 3, we are focusing on an one-sided clamped Euler-Bernoulli rod with boundary conditions at $s = 0$:

$$\left.\begin{aligned} x(0) &= 0 \\ y(0) &= 0 \\ \varphi(0) &= 0 \end{aligned}\right\} \tag{2}$$

Applying a static force load F at $s = s_F$ under angle α to the undeformed rod, there are two possibilities of acting: *direction preserving (dp)* or *angle preserving (ap)*[1] load, see Fig. 4.

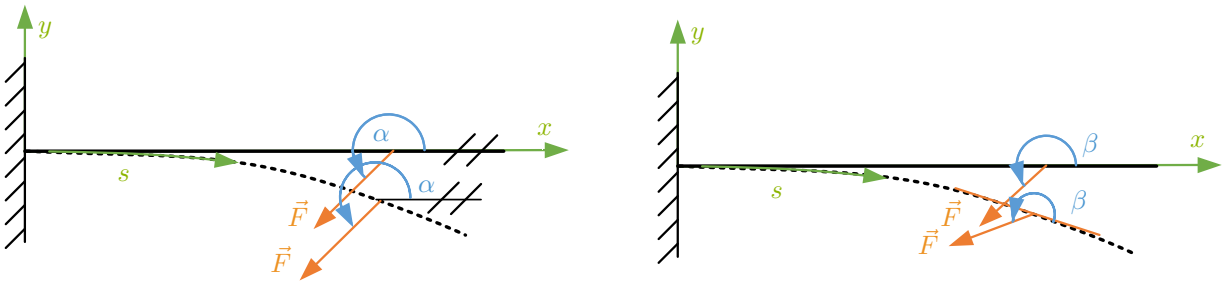

Figure 4. Load scenarios: direction preserving (left), angle preserving (right).

Then, the corresponding bending moments w.r.t the z-axis are:

$$M_{bz_{dp}}(s) = \begin{cases} F\, \sin(\alpha)\, \Big(x(s_F) - x(s)\Big) - F\, \cos(\alpha)\, \Big(y(s_F) - y(s)\Big)\,, & s \in (0, s_F) \\ 0\,, & s \in (s_F, L) \end{cases} \tag{3}$$

$$M_{bz_{ap}}(s) = \begin{cases} F\, \sin\Big(\beta + \varphi(s_F)\Big)\, \Big(x(s_F) - x(s)\Big) - F\, \cos\Big(\beta + \varphi(s_F)\Big)\, \Big(y(s_F) - y(s)\Big)\,, & s \in (0, s_F) \\ 0\,, & s \in (s_F, L) \end{cases} \tag{4}$$

Now, we introduce the conicity of the rod, to have a well-defined set of equations (1). Following the remarks on the conicity in Section 1, we analyze a conically shaped rod with a linear decreasing diameter from base to tip [24].

[1] In the dp-case, the force has constant x- and y-coordinates in the undeformed and deformed state, whereas in ap-case the force has always the same angle β to the tangent of the deformed rod.

For this, we introduce the diameter function

$$d(s) = d(0) - a\,\frac{d(0)}{L}\,s,\ s \in [0, L]\,,\ \text{with } a := 1 - \frac{d(L)}{d(0)}\,, \tag{5}$$

whereas a is now a design factor:

- $a = 0 \Rightarrow d(L) = d(0)$, we have a cylindrical shape,
- $a < 1 \Rightarrow d(L) > 0$, we have a truncated cone,
- $a \approx 1 \Rightarrow d(L) \approx 0$, we have a hastate conical rod, see Fig. 5.

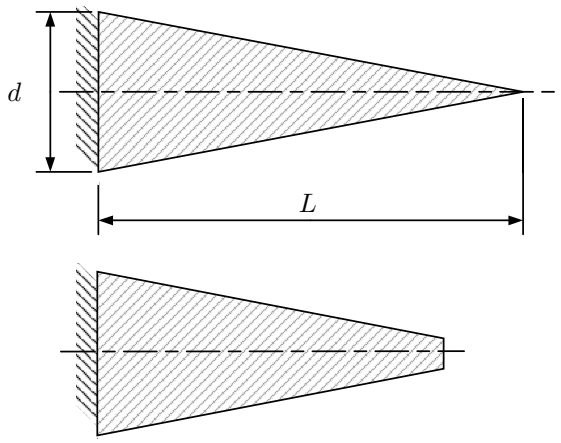

Figure 5. Model of the rod with linearly changing diameter: hastate conical rod (top) and truncated cone (bottom).

Remark 1. *It is easy to introduce such a function* (5) *for an inner diameter if the cone is hollow.*

Then, the second moment of area becomes

$$I_z(s) = \frac{\pi}{64}\,d(s)^4, \text{ for } s \in [0, L]. \tag{6}$$

Remark 2. *For upcoming investigations the following dimensioning is suitable. We introduce the units*

$$[\textit{length}] := L\,, \quad [\textit{force}] := \frac{E\,I_z(0)}{L^2}\,, \quad [\textit{moment}] := \frac{E\,I_z(0)}{L}\,,$$

with L as the length, E as Young's modulus, and $I_z(0)$ as the second moment of area at $s = 0$ of the rod. Fron now on, all quantities are represented dimensionless.

Using the units from Remark 2 and (6), there arise the following sets of equations:

direction preserving-case:

for $s \in [0, s_F]$

$$\begin{aligned}
\frac{dx_1}{ds} &= \cos\Big(\varphi_1(s)\Big) && ,x_1(0) = 0\\
\frac{dy_1}{ds} &= \sin\Big(\varphi_1(s)\Big) && ,y_1(0) = 0\\
\frac{d\varphi_1}{ds} &= f\,\frac{\sin(\alpha)\,\Big(x_1(s_F) - x_1(s)\Big) - \cos(\alpha)\,\Big(y_1(s_F) - y_1(s)\Big)}{\big(1 - a\,s\big)^4} && ,\varphi_1(0) = 0
\end{aligned} \tag{7}$$

for $s \in (s_F, 1]$

$$\begin{aligned}
\frac{dx_2}{ds} &= \cos\Big(\varphi_2(s)\Big) && ,x_2(s_F-) = x_2(s_F+)\\
\frac{dy_2}{ds} &= \sin\Big(\varphi_2(s)\Big) && ,y_2(s_F-) = y_2(s_F+)\\
\frac{d\varphi_2}{ds} &= 0 && ,\varphi_2(s_F-) = \varphi_2(s_F+)
\end{aligned}$$

System (7) forms a 2-point boundary-value problem with **two** unknown quantities $x_1(s_F)$ and $y_1(s_F)$.

$$
\begin{aligned}
&\underline{\text{angle preserving-case:}}\\
&\text{for } s \in [0, s_F]\\
&\frac{dx_1}{ds} = \cos\Big(\varphi_1(s)\Big) && , x_1(0) = 0\\
&\frac{dy_1}{ds} = \sin\Big(\varphi_1(s)\Big) && , y_1(0) = 0\\
&\frac{d\varphi_1}{ds} = f\,\frac{\sin\Big(\beta+\varphi_1(s_F)\Big)\Big(x_1(s_F)-x_1(s)\Big) - \cos\Big(\beta+\varphi_1(s_F)\Big)\Big(y_1(s_F)-y_1(s)\Big)}{\big(1-a\,s\big)^4} && \\
& && , \varphi_1(0) = 0\\
&\text{for } s \in (s_F, 1]\\
&\frac{dx_2}{ds} = \cos\Big(\varphi_2(s)\Big) && , x_2(s_F-) = x_2(s_F+)\\
&\frac{dy_2}{ds} = \sin\Big(\varphi_2(s)\Big) && , y_2(s_F-) = y_2(s_F+)\\
&\frac{d\varphi_2}{ds} = 0 && , \varphi_2(s_F-) = \varphi_2(s_F+)
\end{aligned}
\tag{8}
$$

System (8) forms a 2-point boundary-value problem with **three** unknown quantities $x_1(s_F)$, $y_1(s_F)$ and $\varphi_1(s_F)$. The systems (7) and (8) are now solved numerically using shooting methods to determine the unknown quantities. Elaborate parameter studies are performed to determine the bending behavior of the rod in dependence on several parameters, e.g. load f, point of application s_F, diameter ratio $\frac{d(1)}{d(0)}$. Exemplarily, the influence of the load f on the bending behavior is shown in Fig. 6.

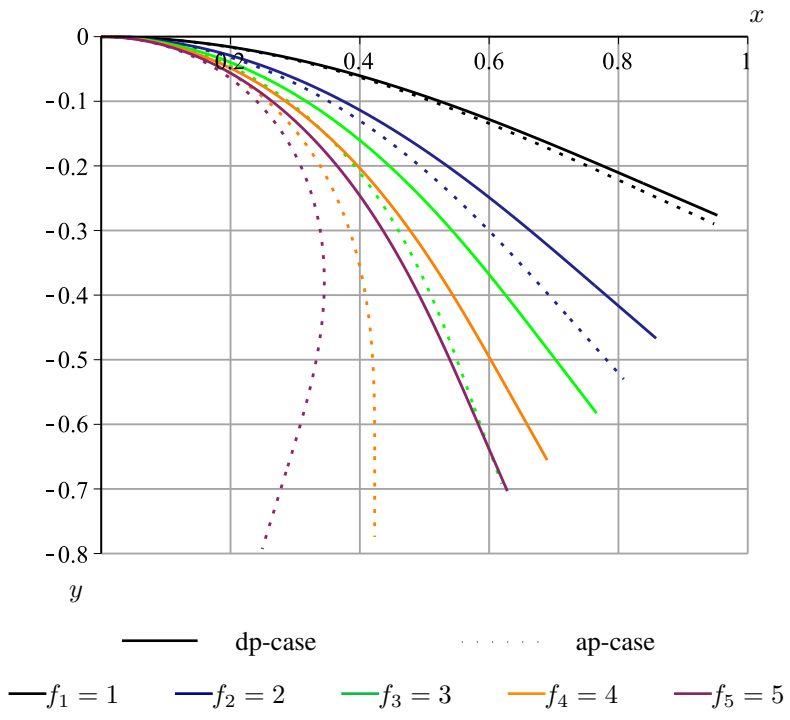

Figure 6. Deformed conically shaped rods (dp- and ap-case) in dependence on load f (using: $a = 0.3$, $s_F = 7/8$ and $\alpha, \beta = 3/2\pi$)

The larger the load, the larger the deflection of the rod, more distinct in the ap-case than the in the dp-one. The dependence on the tapering ratio is shown in Fig. 7. Here, we plot the tip displacement of the rod after applying several loads in dependence on the tapering ratio $\frac{d(1)}{d(0)}$.

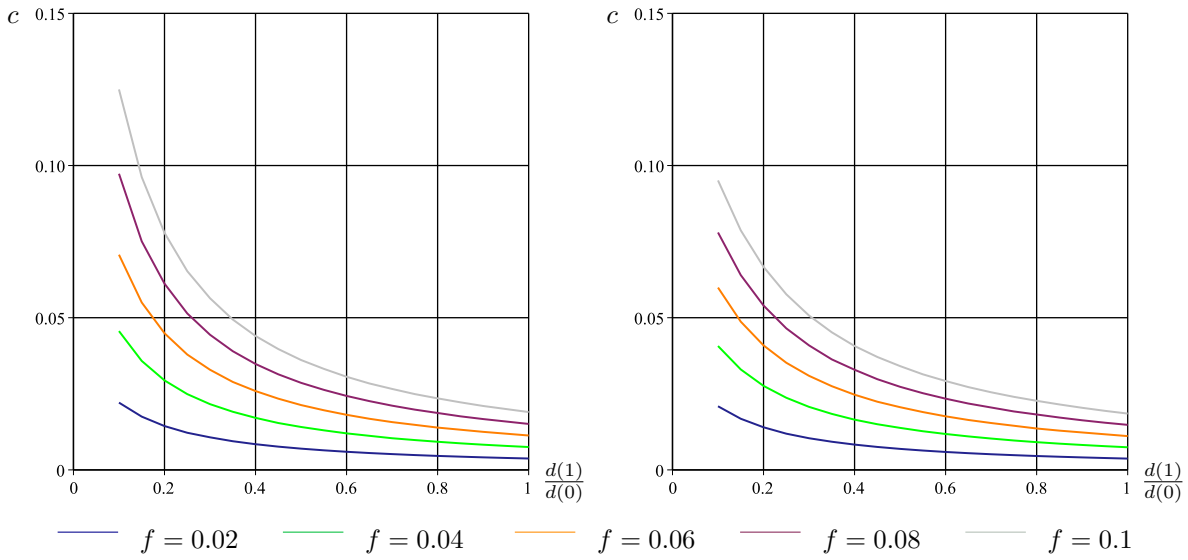

Figure 7. Tip displacement c (using Euklidean norm) of the initial and deformed state of a rod in dependence on $d(1)/d(0)$ for the dp-case (left) and the ap-one (right).

The smaller this ratio, the larger is the tip displacement – in both cases, whereas the dp-case is more related to application in form of object contour detection, which is addressed to the next section.

3. OBJECT CONTOUR DETECTION

After the preliminary studies in Section 2 where the applied force $\vec{F}$ or f, resp., is known, we now switch to an important application of sinus hair-like tactile sensors: object contour detection. For this, we proceed with a modeling section before presenting numerical investigations of the sensing behavior in dependence on the tapering ratio.

3.1. Modeling

Let us consider an one-sided clamped Euler-Bernoulli rod as a mechanical model for object contour/shape detection, as depicted in Fig. 8.

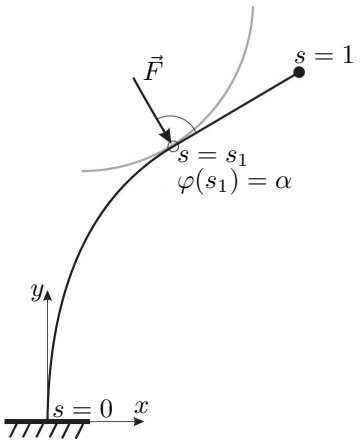

Figure 8. Deformed sinus hair during object sensing.

Let us state the following assertion and assumptions:

- The considered object is assumed to be rigid, has a plane boundary $\Big(\xi(\alpha), \eta(\alpha)\Big)$, represented by a strictly convex function and is parameterized by its slope angle $\alpha \in \Big(-\frac{\pi}{2}, \frac{\pi}{2}\Big)$.
- The artificial sinus hair/rod is moved from the right to left along a horizontal straight line, i.e., we have a moving clamping support[2] at $y = 0$ in negative x-direction.
- The translational velocitiy is nearly zero, i.e., we can consider the problem quasi-statically.
- Due to a contact of the rod to the object, the arising bending of the sinus hair takes place, w.l.o.g., in the x-y-plane.
- The deformation of the rod is linear elastically due to Hooke's law of elasticity.
- The contact (between rod and object at s_1) is assumed to be ideal, i.e., the arising contact force is perpendicular to the profile tangent. Furtheron, we do not take any frictional effects into account.
- The strict convexity of the profile results in the existing of only one contact point at each position of the sinus hair.

3.2. Step 1: Generation of Observables

This step can be skipped if we replace it with an experimental setup and measurements. But, obviously, we will get no analytical insight, therefore, we try to handle this step in an analytical way. The general task here is to determine the clamping reactions for a reconstruction – the quantities an animal solely relies on in nature.
Once again, the starting point is system (1) with diameter (5) and second moment of area (6). The bending moment arises from Fig. 8:

$$m_{bz}(s) = \begin{cases} f\,\left[(\eta(\alpha) - y(s))\,\sin(\alpha) + (\xi(\alpha) - x(s))\,\cos(\alpha)\right]\,, & s \in (0, s_1) \\ 0\,, & s \in (s_1, 1) \end{cases} \tag{9}$$

Before solving the arising equations, we have to point out, that there exist two contact scenarios of the rod with the object, see Fig. 9:

- Phase A: rod tip contact with the object – no information about $\varphi(s_1) = \varphi(1)$, only $s_1 = 1$;
- Phase B: tangentially contact of the rod with the object at $s_1 < 1$ with $\varphi(s_1) = \alpha$.

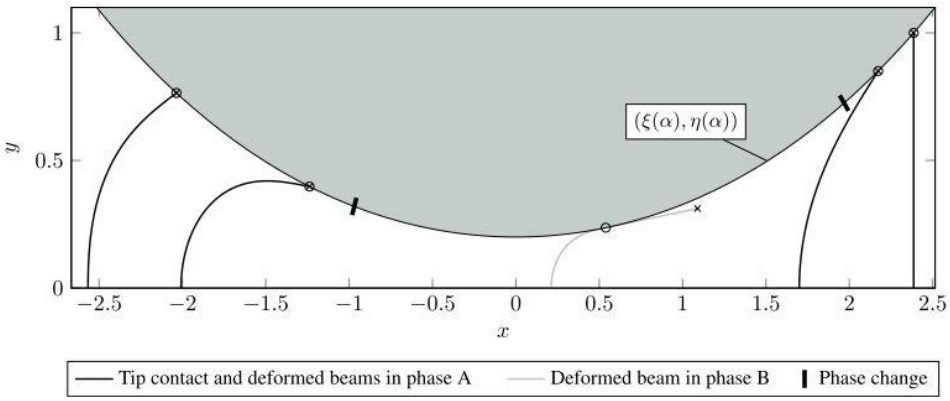

Figure 9. Phases during object sensing (grey - Phase B, and black - Phase A) [25].

Using the dimensioning procedure of Section 2, there arise two systems – not depending on the kind of the preserved quantity, here, depending on the contact phase.

[2] Although we know that there is a certain elasticity at the support of the sinus hair, we assume a clamping for the first investigations. The elasticity is addressed to further studies.

Remark 3. *Due to the fact, that s_1 is unknown, but this is the only point defining the set of equations in Phase B, we introduce a new parameter for the rod length in this case:*

$$s = \tau\, s_1 \tag{10}$$

This will lead to the following two sets of 2-point boundary-value problems with unknown quantities:

- **Phase B**

$$\left.\begin{array}{rcl} \frac{dx(\tau)}{d\tau} &=& s_1\, \cos\big(\varphi(\tau)\big) \\ \frac{dy(\tau)}{d\tau} &=& s_1\, \sin\big(\varphi(\tau)\big) \\ \frac{d\varphi(\tau)}{d\tau} &=& s_1\, \kappa(\tau) \\ \kappa(\tau) &=& \begin{cases} \dfrac{f\,\Big[\big(\eta(\alpha)-y(\tau)\big)\sin(\alpha)+\big(\xi(\alpha)-x(\tau)\big)\cos(\alpha)\Big]}{\big(1-a_1 s_1 \tau\big)^4}, & \text{for } \tau \in [0,1] \\ 0, & \text{for } \tau \in \left(1, \frac{1}{s_1}\right] \end{cases} \end{array}\right\} \tag{11}$$

  with boundary conditions

$$\left.\begin{array}{lcllcl} y(0) &=& 0 \qquad \varphi(1) = \alpha & x(1) &=& \xi(\alpha) \\ \varphi(0) &=& \frac{\pi}{2} & y(1) &=& \eta(\alpha) \end{array}\right\} \tag{12}$$

- **Phase A** (with $s_1 = 1$)

$$\left.\begin{array}{rcl} \frac{dx(\tau)}{d\tau} &=& \cos\big(\varphi(\tau)\big) \\ \frac{dy(\tau)}{d\tau} &=& \sin\big(\varphi(\tau)\big) \\ \frac{d\varphi(\tau)}{d\tau} &=& \kappa(\tau) \\ \kappa(\tau) &=& \dfrac{f\,\Big[\big(\eta(\alpha)-y(\tau)\big)\sin(\alpha)+\big(\xi(\alpha)-x(\tau)\big)\cos(\alpha)\Big]}{\big(1-a_1\tau\big)^4} \end{array}\right\} \tag{13}$$

  with boundary conditions

$$\left.\begin{array}{lcllcl} y(0) &=& 0 & x(1) &=& \xi(\alpha) \\ \varphi(0) &=& \frac{\pi}{2} & y(1) &=& \eta(\alpha) \end{array}\right\} \tag{14}$$

In applying shooting methods to these systems, we are able to determine the unknown quantities f and s_1.

Remark 4. *As in Section 1, the animal solely relies on the information of the mechanoreceptor cells in the follicle-sinus complex. Hence, we have to determine the clamping reactions for a reconstruction, although we have determined s_1.*

Following up, we get the clamping reactions:

$$f_{Ax} = -f\, \sin(\alpha)\,, \quad f_{Ay} = f\, \cos(\alpha)\,, \quad m_{Az} = -m_{bz}(0+)\,.$$

If we now move the base support by an increment Δx_0 to the right, i.e., we are changing the actual position x_0 (or changing the consideration to the slope angle α) the complete calculation starts again (a loop), which results in functions:

$$f_{Ax} = f_{Ax}(x_0)\,, \quad f_{Ay} = f_{Ay}(x_0)\,, \quad m_{Az} = m_{Az}(x_0)$$

Exemplarily, Fig. 10 presents the clamping reactions while scanning a convex profile $x \mapsto g(x) = x^2 + 0.3$ with an artifical vibrissa using various tapering ratios. Having a closer look to the subfigures of Fig. 10, one can observe two facts:

- At first, no information about the profile contour can be extracted from the clamping reactions, but
- for smaller tapering ratios $\frac{d(1)}{d(0)}$, i.e., higher desgin factors a, remind (5), all clamping reactions can be decreased – up to limits of measurements.

The first assertion yields the claim for a reconstruction algorithm.

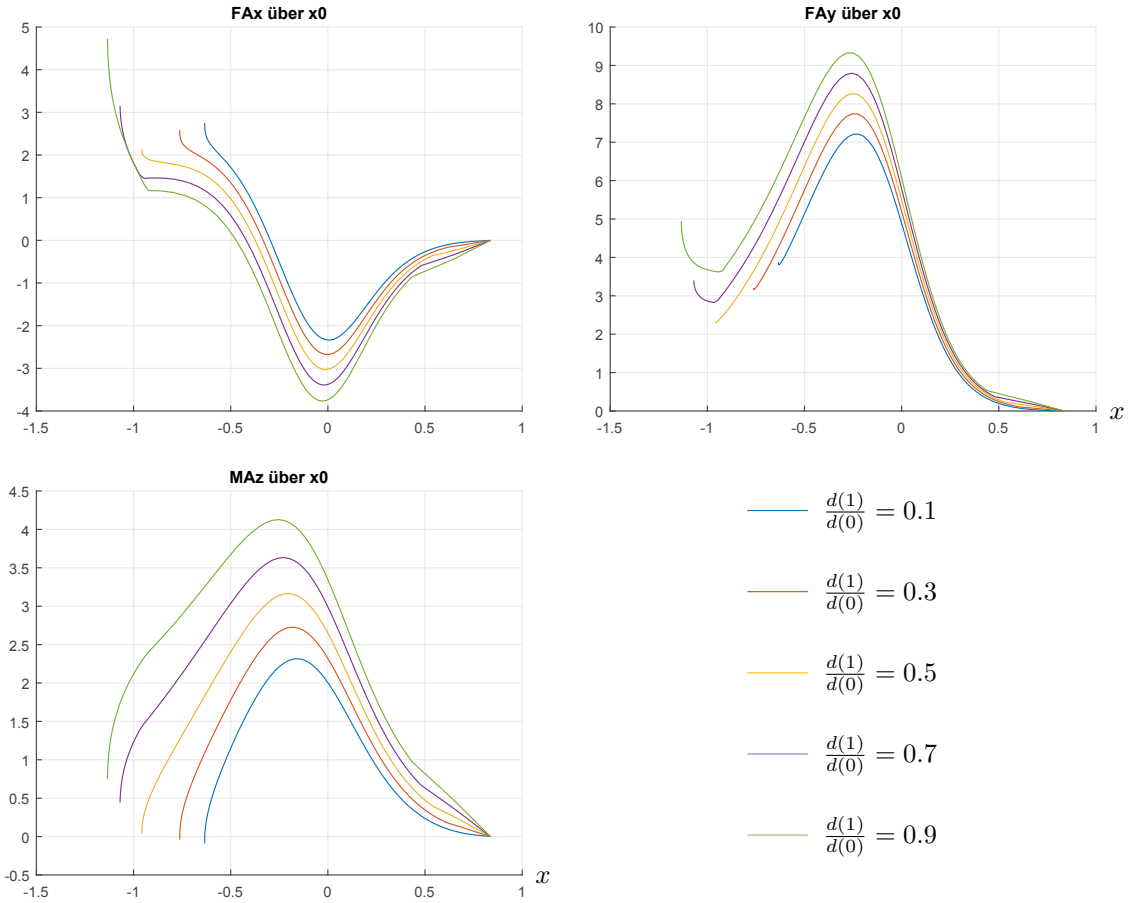

Figure 10. Clamping reactions f_{Ax} (top left), f_{Ay} (top right), moment m_{Az} (bottom) during object sensing using a parabola profile $g(x) = x^2 + 0.3$ for different vibrissa tapering ratios.

3.3. Step 2: Contour Reconstruction

Now, we have the following quantities at hand:

- the clamping reactions from Step 1 or measured in experiments, and
- the base position x_0.

Using these quantities, we are able to determine

$$f = \sqrt{{f_{Ax}}^2 + {f_{Ay}}^2} \quad \text{and} \quad \alpha = \arctan\left(-\frac{f_{Ax}}{f_{Ay}}\right)$$

which were used in the previous sets of equations.
The main idea now is, contrary to Step 1 in solving a boundary-value problem with unknowns, to solve an initial-value problem. This is possible, since the bending moment is fully known using a positive cut applying method of sections, see Fig. 11:

$$m_{bz}(s) = -m_{Az} + f_{Ay}\left(x(s) - x_0\right) - f_{Ax}\, y(s)\,. \tag{15}$$

The initial-value problem – to be solved until $m_{bz} = 0$ – is now:

$$\left.\begin{aligned} \frac{dx(s)}{ds} &= \cos\left(\varphi(s)\right) && ,x(0) = x_0 \\ \frac{dy(s)}{ds} &= \sin\left(\varphi(s)\right) && ,y(0) = 0 \\ \frac{d\varphi(s)}{ds} &= \kappa(s) = -m_{Az} + f_{Ay}\left(x(s) - x_0\right) - f_{Ax}\, y(s) && ,\varphi(0) = \frac{\pi}{2} \end{aligned}\right\} \tag{16}$$

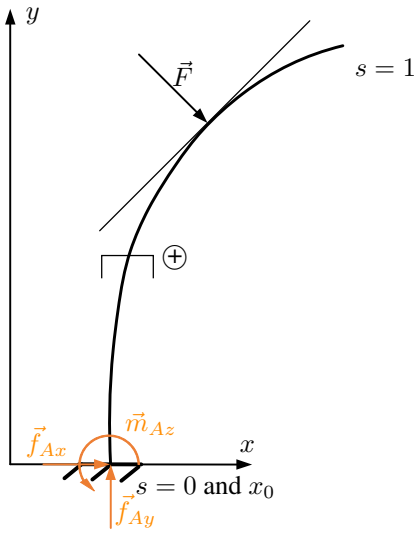

Figure 11. Applying method of sections to determine the bending moment.

3.4. Numerical Simulation

Here, we sense an object with a profile boundary mentioned before $g(x) = x^2 + 0.3$, using several tapering ratios, see Fig. 12.

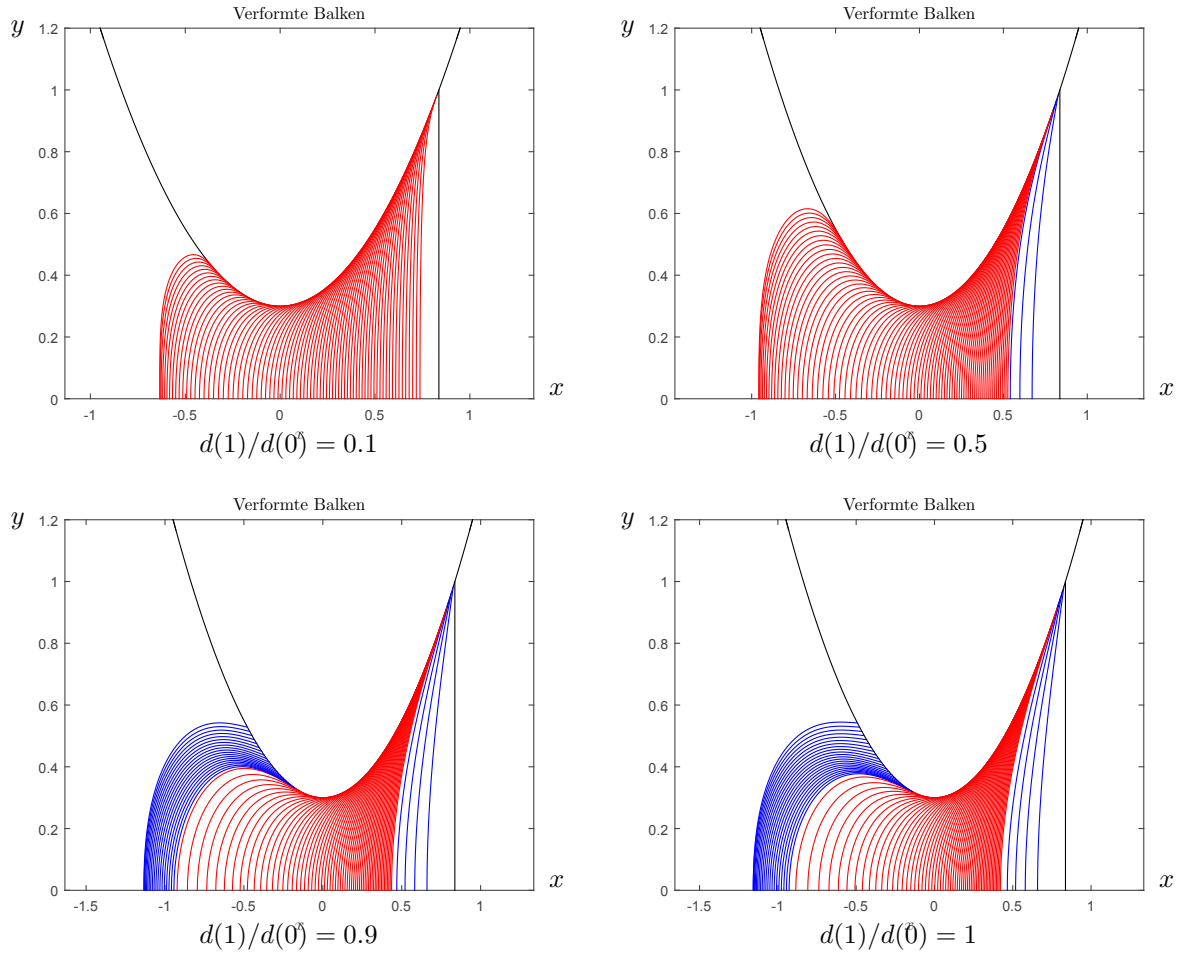

Figure 12. Deformed vibrissae while scanning the profile boundary $g(x) = x^2 + 0.3$ using several tapering ratios $d_{al}(1)/d_{al}(0)$ (red - contacting in Phase B, blue - contacting in Phase A).

To judge the quality of reconstruction we introduce a reconstruction error between actual point of the profile contour and the reconstructed one, according to [25]:

$$\text{error} = \sqrt{\Big(x(s_1) - \xi(\alpha)\Big)^2 + \Big(y(s_1) - \eta(\alpha)\Big)^2}.$$

For our simulation results, we get the error displayed in Fig. 13.

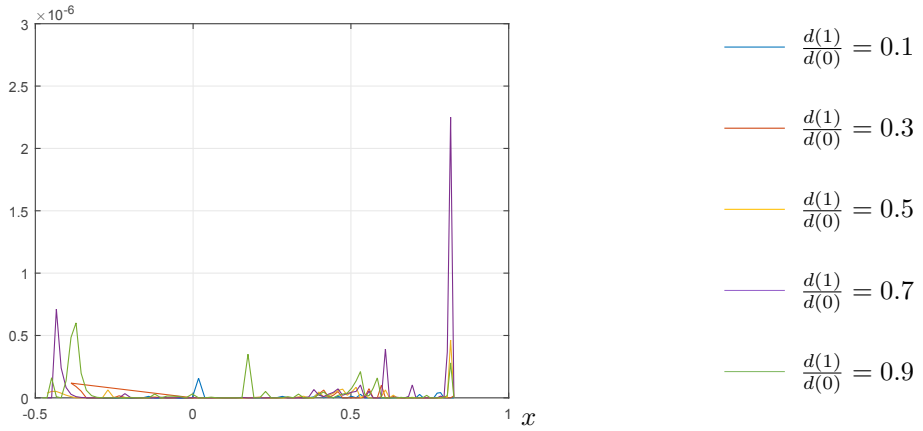

Figure 13. Reconstruction error in numerical simulations.

For larger tapering ratios we get higher reconstruction error, but the errors for the used tapering ratios are of order 10^{-6}.

4. CONCLUSIONS & OUTLOOK

Bionic researches of sensors and actuators persue the objective to use the advantages and properties of the natural vibrissa for technical innovations. For this, a detailed knowledge about the bending behavior is essential. This paper was devoted to the analytical investigation of sinus hair-like tactile sensors using Euler-Bernoulli rods which exhibit a conical shape. The investigations were inspired by the natural geometrical shape of the biological paradigm. Most papers in literature focused on cylindrically shaped rods for object contour detection or use approximation models as multi-body and/or finite element ones. Therefore, we investigated the bending behavior of a one-sided clamped cylindrical sinus hair that was then extended to a conical shape (here, we focused on a linearly decreasing diameter from tip to base). Based on the models, the corresponding differential equations were derived. The static bending behavior depending on different geometry parameters was analyzed and discussed. The simulation results showed a strong impact of the conicity of a sinus hair on the bending behavior in comparison with cylindrical ones. Then, a model to simulate the object scanning by using a technical sinus hair was expanded to a conical geometry. In this context, the observables and the relative error for the reconstructed profile were calculated and analyzed. At this point, observables are the support reactions at the clamp, which could be measured in experiments. The results showed that a conical geometry has a large impact on the generated observables. In contrast, the relative error of the reconstructed profile is hardly changed.

Future work shall encompass

- investigations of the bending behavior with respect to other conical shapes: exponentially changing diameter, hollow profiles;
- incorporation of friction during contact;
- extending the sensing model to a rotational movement of the vibrissa instead of a translational movement of the support, which is then more realistic to nature.

5. REFERENCES

[1] Ahl A.S. (1986): The role of vibrissae in behavior: a status review; *Veterinary Research Communications* 10(4): 245–269.

[2] Behn C., Schmitz T.A., Witte H., Zimmermann K. (2013): Animal vibrissae: modelling and adaptive control of bio-inspired sensors; in: *Proceedings IWANN 2013*, Eds.: Rojas I., Joya G., Cabestany, J., Springer, 159-–170.

[3] Behn C. (2013a): Modeling the Behavior of Hair Follicle Receptors as Technical Sensors using Adaptive Control; in: *Proceedings of 10th International Conference on Informatics in Control, Automation and Robotics* (ICINCO 2013), Reykjavík (Iceland), pp. 336-345, SciTePress, DOI:10.5220/0004488003360345.

[4] Belli H.M., Yang A.E.T. Bresee C.S., Hartman M.J.Z. (2017): Variations in vibrissal geometry across the rat mystacial pad: base diameter, medulla, and taper; *Journal of Neurophysiology* 117(4): 1807—1820.

[5] Bhuta P.G. (1964): Exact nonlinear solution of the bending of a constrained beam; *Zeitschrift für angewandte Mathematik und Physik* 6: 647—652.

[6] Brecht M., Preilowski B., Merzenich M.M. (1997): Functional architecture of the mystacial vibrissae; *Behavioural Brain Research* 84: 81—97.

[7] Carvell G.E., Simons D.J. (1990): Biometric analyses of vibrissal tactile discrimination in the rat; *The Journal of Neuroscience* 10(8): 2638-–2648.

[8] Dehnhardt G., Kaminski A. (1995): Sensitivity of the mystacial vibrissae of harbour seals phocavitulina for size differences of actively touched objects; *The Journal of Experimental Biology* 198: 2317—2323.

[9] Ebara S., Kumamoto K., Matsuura T., Mazurkiewicz J.E., Rice F.L. (2002): Similarities and differences in the innervation of mystacial vibrissal follicle-sinus complexes in the rat and cat: A confocal microscopic study; *The Journal of Comparative Neurology* 449(2): 103-–119.

[10] Hartman M.J.Z., Johnsin N.J., Blythe T.R., Assad C. (2003): Mechanical Characteristics of Rat Vibrissae: Resonant Frequencies and Damping in Isolated Whiskers and in the Awake Behaving Animal; *Journal of Neuroscience* 23(16): 6510-–6519.

[11] Helbig T., Zárate J., Voges D., Behn C., Witte H. (2017): Mechanical bearings with tunable compliance – the follicle-sinus-complex as paragon; in: *Bionik: Patente aus der Natur*, Eds.: Kesel A.B., Zehren D., Bremen: 261-–267.

[12] Hires S.A., Pammer L., Svoboda K., Golomb D. (2013): Tapered whiskers are required for active tactile sensation; *eLife* 2(0): e01350.

[13] Jenks R.A. (2007): Mechanical and neural representations of tactile information in the awake behaving rat somatosensory pathway; PhD thesis, Department of Physics, Harvard University, Cambridge.

[14] Löbel G. (1963): Große Biegeverformungen bei schlanken geraden und kreisförmigen Trägern; *Zeitschrift für Angewandte Mathematik und Mechanik* 43(1-2): 25-–46.

[15] Long S.Y. (1972): Hair-nibbling and whisker-trimming as indicators of social hierarchy in mice; *Animal Behaviour* 20(1): 10—12.

[16] Neimark M.A., Andermann M.L., Hopfield J.J., Moore C.I. (2003): Vibrissa Resonance as a Transduction Mechanism for Tactile Encoding; *Journal of Neuroscience* 23(16): 6499-–6509.

[17] Quist B.W., Hartman M.J.Z. (2012): Mechanical signals at the base of a rat vibrissa: the effect of intrinsic vibrissa curvature and implications for tactile exploration; *Journal of Neurophysiology* 107(9): 2298-–2312.

[18] Schmidt M., Witte H., Zimmermann K., Niederschuh S., Helbig T., Voges D., Husung I., Volkova T., Will C., Behn C. (2014): Technical, non-visual characterization of substrate contact using carpal vibrissae as a biological model: an overview; in: *Proceedings of 58th International Scientific Colloquium – Shaping the future by engineering*, September 2014, Ilmenau, Germany.

[19] Scholz G.R., Rahn, C.D. (2004): Profile Sensing With an Actuated Whisker; *IEEE Transactions on Robotics and Automation* 20(1): 124-–127.

[20] Shatz L.F., de Groot T., Aegerter C.M. (2013): The Frequency Response of the Vibrissae of Harp Seal, Pagophilus Groenlandicus, to Sound in Air and Water; *PLoS ONE* 8(1): e54876.

[21] Sokolov V.E., Kulikov V.F. (1987): The structure and function of the vibrissal apparatus in some rodents; *Mammalian Species* 51(1): 125-–138.

[22] Steigenberger J. (2013): A continuum model of passive vibrissae; Preprint No. M13/03, Institute of Mathematics, TU Ilmenau, Germany.

[23] Vocke W. (1964): Die elastische Biegung des Balkens bei großer Verformung; *Zeitschrift für Angewandte Mathematik und Mechanik* 44(3): 119-–122.

[24] Voges D., Carl K., Klauer G.J., Uhlig R., Schilling C., Behn C., Witte H. (2012): Structural Characterization of the Whisker System of the Rat; *IEEE Sensors Journal* 12(2): 332-–339.

[25] Will C., Steigenberger J., Behn C. (2014): Object Contour Reconstruction using Bio-inspired Sensors; in: *Proceedings of the 11th International Conference on Informatics in Control, Automation and Robotics (ICINCO)*, Springer, pp. 459-–467.

[26] Williams C.M., Kramer E.M., Scalas E. (2010): The Advantages of a Tapered Whisker; *PLoS ONE* 5(1): e8806.

[27] Witte H., Schilling C. (2017): The Concept of Biomechatronic Systems as a Means to Support the Development of Biosensors; *International Journal of Biosensors & Bioelectronics* 2(4):00030.

[28] Yan W., Kan Q., Kergrene K., Kang G., Feng X.-Q., Rajan R. (2013): A truncated conical beam model for analysis of the vibration of rat whiskers; *Journal of Biomechanics* 46(12): 1987-–1995.

[29] Yanli B., Wei Z., Yanchun X., Jun Z., Xiaoming T. (1998): Relationship between structure and function of mammalian vibrissa; *Journal of Forestry Research* 9(4): 273-–282.

[30] Yu Y.S.W., Graff M.M., Bresee C.S., Man Y.B., Hartman M.J.Z. (2016): Whiskers aid anemotaxis in rats; *Science Aadvances* 2(8): e1600716.